

## Heat capacity of solid $^4\text{He}$ and $^3\text{He}$ - $^4\text{He}$ mixture grown in aerogel

Zhi Gang Cheng,<sup>1</sup> Norbert Mulders,<sup>2</sup> and Moses H. W. Chan<sup>1,\*</sup>

<sup>1</sup>*Department of Physics, The Pennsylvania State University, University Park, Pennsylvania 16802, USA*

<sup>2</sup>*Department of Physics and Astronomy, University of Delaware, Newark, Delaware 19716, USA*

(Received 8 October 2014; revised manuscript received 17 November 2014; published 1 December 2014)

We report heat capacity measurements of solid  $^4\text{He}$  and  $^3\text{He}$ - $^4\text{He}$  solid mixture samples grown in silica aerogel. In addition to the Debye  $T^3$  term, the heat capacity of solid  $^4\text{He}$  samples includes  $T$  linear and  $T^2$  terms which are attributed to the amorphous and two-dimensional helium layers confined near the silica strands of aerogel. Beside these regular polynomial terms, a broad heat capacity peak is found between 0.1 and 0.35 K. The peak probably has its origin in the vibration of the dislocation lines pinned by the silica strands. Compared to  $^4\text{He}$  samples, the heat capacity of solid  $^3\text{He}$ - $^4\text{He}$  mixture samples shows evidence of phase separation below a characteristic temperature  $T_c$  that increases with  $^3\text{He}$  concentration ( $X_3$ ). Below this temperature the heat capacity shows  $X_3^{1/2}$  dependence suggesting that the  $^3\text{He}$  atoms are phase separated from being uniformly distributed in the pore space into two-dimensional patches enfolding the silica strands that are themselves coated with a strongly bound amorphous  $^4\text{He}$  layer.

DOI: [10.1103/PhysRevB.90.224101](https://doi.org/10.1103/PhysRevB.90.224101)

PACS number(s): 67.80.-s, 67.60.-g, 61.72.-y

### I. INTRODUCTION

In 2004, Kim and Chan carried out torsional oscillator (TO) experiments of solid  $^4\text{He}$  both in porous Vycor [1] and in bulk space [2] and observed an abrupt drop in the resonant period of the TO below 0.2 K. This phenomenon was interpreted as possible evidence of missing or nonclassical rotational inertia (NCRI) and evidence of supersolidity. Since the initial observations, this behavior has been replicated in 30 other TO experiments in 11 laboratories [3–13]. There was early evidence suggesting that the size of NCRI is dependent on the crystalline quality of the sample and disordered polycrystalline samples exhibit larger supersolid fractions than single-crystal samples. The results of a combined x-ray scattering and TO experiment on solid helium grown in aerogel of 95% porosity [14], however, are not consistent with this premise. Specifically while the x-ray scattering results show the solid helium sample in aerogel to be polycrystalline with crystalline grain size of only 100 nm, TO measurements found a small apparent NCRI of  $4 \times 10^{-4}$ , similar to that found in single-crystal samples [14].

On the other hand the shear modulus of solid helium at low temperatures showed a very significant increase that has the same onset temperature and shows identical temperature and  $^3\text{He}$  concentration dependencies as the purported NCRI signature [15]. The low-temperature shear modulus value showed an enhancement that ranges between 10% and 80% to that found above the onset temperature. The increase was interpreted as the result of the stiffening of dislocation lines due to the binding of  $^3\text{He}$  impurities [15,16]. It can be shown that the abrupt stiffening of solid helium can also lead to a period drop in the TO [17,18]. The resultant drop in resonant period can be very substantial if the TOs are not rigid. Conversely, this effect can be minimized in a rigid TO. Recent TO experiments on bulk solid samples housed in particularly rigid TOs found either very small period drops or no period drop within the resolution of the experiments. These experiments

found upper limits of NCRI that range from  $4 \times 10^{-6}$  to  $3 \times 10^{-5}$  [19,20]. In a new TO experiment with solid helium in Vycor where bulk solid helium is completely eliminated, no NCRI signal within experimental resolution ( $2 \times 10^{-5}$ ) was observed [21]. These results indicate that the period drops previously observed in TOs are most likely consequence of the shear modulus stiffening of the bulk solid helium and not evidence of supersolidity.

In 2007, the heat capacity of bulk solid  $^4\text{He}$  in a silicon sample cell was measured [22]. A peak centering near 90 mK in addition to the  $T^3$  Debye contribution was found. The peak was interpreted as the possible thermodynamic signature of NCRI because its temperature is close to the onset temperature of the purported NCRI. The peak size is, however, extremely small,  $\sim 6 \times 10^{-6} k_B$  per  $^4\text{He}$  atom. In more recent measurements [23,24], a peak was found at lower temperature and the sizes were  $\sim 10$  times smaller for samples grown between sapphire disks and in coexistence with liquid. In view of the most recent results from TO experiments that cast strong doubts on the existence of supersolidity in solid helium, there is uncertainty on the physical origin of the heat capacity peak. There is a renewed effort in determining whether the peak is an instrumental effect related to unaccounted heat leaks to the calorimeter or the less than perfect measurement condition requiring long external and short internal thermal equilibration times for the calorimeter. The results of this effort will be published in a separate paper [25].

In this paper, we report a heat capacity study of solid helium in silica aerogel of 95% porosity, similar to that used in the combined x-ray and TO experiment [14]. This experiment was initiated in 2010 to search for the heat capacity peak similar to that reported in bulk solid helium samples [22–24] in order to gain insight into the physical origin of the peak. While we did not find any evidence that can be unambiguously attributed to the onset of supersolidity, we found a broad heat capacity peak near 0.22 K marking the excitation of the vibrational state of the dislocation lines that are pinned by the silica strands. To our knowledge this is the first thermodynamic signature of the dislocation network in solid helium. We also found evidence of isotopic phase separation of  $^3\text{He}$ - $^4\text{He}$  solid mixture

\*chan@phys.psu.edu

samples with  $^3\text{He}$  concentrations that range from 6 ppm to 1.4%. Within the resolution of our experiment the heat capacity signature is not hysteretic upon warming and cooling. Below the phase separation temperature the heat capacity shows an  $X_3^{1/2}$  (at fixed  $T$ ) and  $T^2$  (at fixed  $X_3$ ) dependence. The  $X_3^{1/2}$  dependence suggests that at low temperature the  $^3\text{He}$  atoms form two-dimensional (2D) patches phase separated from  $^4\text{He}$  solid. We will show below that this is possible for  $^3\text{He}$ - $^4\text{He}$  mixtures confined inside the silica aerogel network.

Due to the strong  $^4\text{He}$ -silica van der Waals attraction, there is an amorphous layer of  $^4\text{He}$  that is tightly bound to the surface of the silica strands of the aerogel. Since the van der Waals potential drops off rapidly with distance [26], bulklike crystallites are nucleated in the interior of the pore space a few atomic diameters from the silica strands. A path-integral Monte Carlo (PIMC) simulation study of solid  $^4\text{He}$  inside a porous glass [27] found a narrow spatial region sandwiched between the amorphous layer and the bulklike  $^4\text{He}$  crystalline grains in which  $^4\text{He}$  atoms exhibit 2D layered structure. Their simulation showed that the  $^4\text{He}$  layer right above the amorphous layer is less dense than the solid in the crystallites and is superfluid. The existence of a 2D layer is plausible because the screening of the strongly bound amorphous layer improves the smoothness of van der Waals potential in the plane conforming to the substrate surface. As a result the atoms are less localized laterally in this two-dimensional surface layer enclosing the tightly bound amorphous layer. Therefore this layer exhibits 2D-like behaviors. Recent neutron scattering experiments provided evidence for the existence of such layered structure [28]. Our measurements support the presence of such a 2D  $^4\text{He}$  layer. But we found that such layer is solidlike. The PIMC simulation also demonstrated that this intermediate layer provides potential minima for  $^3\text{He}$  atoms to reside at low temperatures [27]. It showed that  $^3\text{He}$  atoms are more evenly distributed across the entire system at high temperature ( $T = 0.7$  K) while they mostly concentrate on this intermediate layer when temperature is lowered ( $T = 0.2$  K). Our results on the  $^3\text{He}$ - $^4\text{He}$  mixture samples found evidence in support of phase-separated 2D  $^3\text{He}$  patches at low temperature. In the following sections, we will describe separately the experimental findings and their significance on solid  $^4\text{He}$  and on the mixtures.

## II. EXPERIMENTAL SETUP

The calorimeter, shown in Fig. 1, is made of single-crystal sapphire to achieve a low heat capacity background. A cylindrical piece of silica aerogel (diameter = 1.42 cm, height = 0.76 cm) is tightly placed in the cavity of the calorimeter. The aerogel piece has a porosity of 95% and a specific surface area of  $\sim 100$  m<sup>2</sup>/cm<sup>3</sup>. Therefore the calorimeter has an open pore volume of 1.14 cm<sup>3</sup> and a surface area of  $\sim 120$  m<sup>2</sup>. There is a very small bulk space free of aerogel in the calorimeter contributed by the fill line and the imperfect match of the aerogel piece to the cavity of the calorimeter. We estimate that this bulk space has a volume of  $\sim 1 \times 10^{-3}$  cm<sup>3</sup>. Neutron and x-ray studies [29,30] show that the microstructure of the aerogel consists of interconnected silica strands of

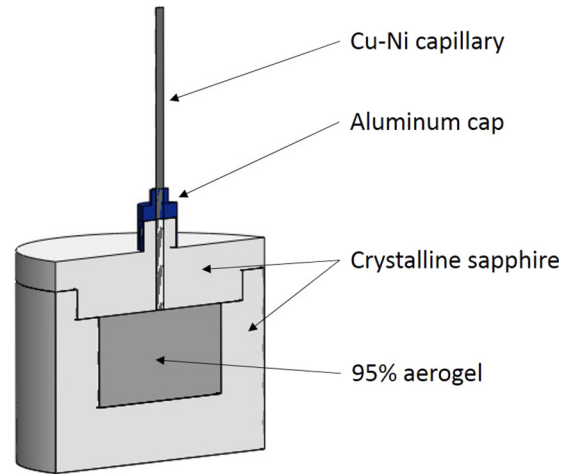


FIG. 1. (Color online) Calorimeter for the heat capacity measurement of solid helium grown in aerogel.

approximately 5 nm in diameter and the strands form a three-dimensional fractal network. Spatial separation between strands is 30  $\sim$  100 nm. The heat capacity measurements are performed with the ac calorimetry method as in the previous heat capacity measurements of bulk solid  $^4\text{He}$  in our laboratory [22–24].

## III. RESULTS ON PURE $^4\text{He}$ SAMPLES

The solid  $^4\text{He}$  samples are prepared with commercially available ultrahigh-purity (UHP)  $^4\text{He}$  gas with  $X_3 = 0.3$  ppm and isotopically pure  $^4\text{He}$  gas with  $X_3 = 1$  ppb. Both samples are made with the blocked capillary method and a final pressure of  $50 \pm 1$  bar. Figure 2(a) shows the measured heat capacities of these samples after subtracting the background heat capacities of the empty calorimeter and other addenda, which account for  $\sim 3\%$  of the total heat capacity. The two data sets are virtually identical indicating that  $^3\text{He}$  impurities at 0.3 ppm level do not play any role in determining the thermal properties of the system and both samples can be considered to be pure  $^4\text{He}$ . As noted above the strong van der Waals potential of the  $\text{SiO}_2$  molecules of the silica strands precipitates an amorphous  $^4\text{He}$  layer. This layer is approximately 2 atomic layers thick and the binding energy for the amorphous layer ranges from 10 to 25 K [26]. Like any other amorphous material, excitations of two-level systems (TLS) exist in the amorphous helium and contribute a heat capacity that scales with  $T$  [31,32]. The crystalline grains in the interior pore space contribute a heat capacity scaling with  $T^3$ . As noted above, a PIMC simulation study shows that there exists a layer of helium that lies between amorphous and crystalline regions [27]. If this is the case, two-dimensional phonons can be excited in this distinct layer and give rise to a heat capacity scaling with  $T^2$ . The measured heat capacity as a function of temperature of both samples shows a broad peak that centers near 0.22 K. In order to display this broad peak more clearly, we fit the regular heat capacity away from the peak region with two different polynomial expressions, one without and the other with the  $T^2$  term:  $C_{\text{fitA}} = a_1 T + a_3 T^3$  and  $C_{\text{fitB}} = a_1 T + a_2 T^2 + a_3 T^3$ . The fitting parameters are

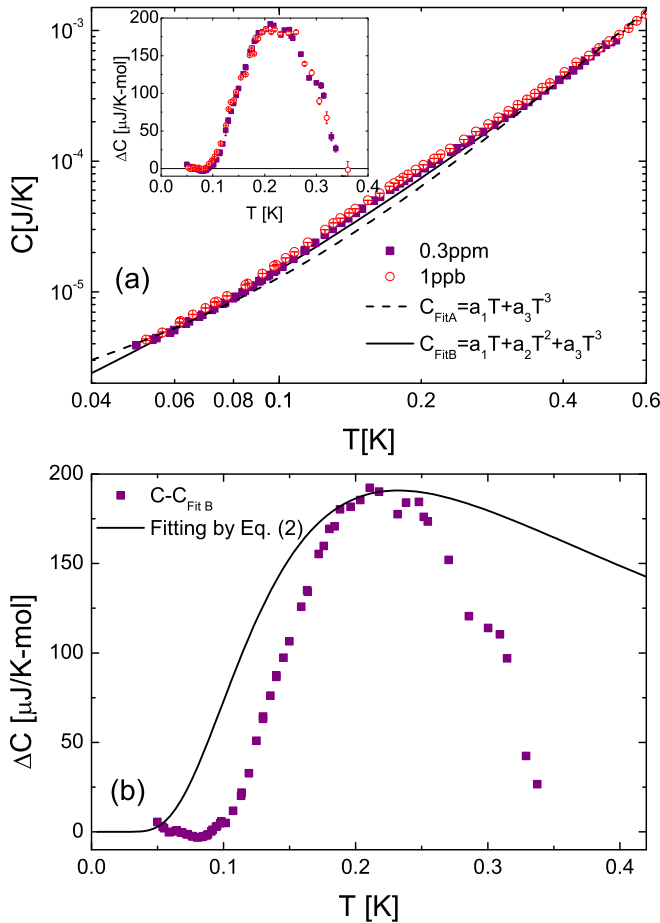


FIG. 2. (Color online) (a) Heat capacity of solid  $^4\text{He}$  samples ( $X_3 = 0.3$  ppm, 1 ppb) grown in aerogel with polynomial fittings A and B. The inset shows the broad heat capacity peak after subtracting fit B. Error bars are smaller than the symbols. (b) Heat capacity peak after subtracting fit B (square) and fitting of the peak by Eq. (2) (solid line).

listed in Table I. It is difficult to tell from Fig. 2(a) which expression provides a better fit for the data away from the peak. However we found that if the  $T^2$  term is omitted (fit A), the coefficient for the  $T^3$  term  $a_3$  is 60% higher than that expected value ( $3854 \mu\text{J/K}^4$ ) for a crystalline solid  $^4\text{He}$  at 50 bars with a Debye temperature of 30 K [33,34]. On the other hand the expression with a  $T^2$  term (fit B) gives a  $T^3$  term that is only 20% higher. An enhanced  $T^3$  term in heat capacity is possible for heavily disordered solids; e.g., amorphous germanium has a  $T^3$  term 50% larger than its crystalline counterpart [35]. Since the solid  $^4\text{He}$  in aerogel is not completely amorphous [14], the 60% enhancement for the  $T^3$  term found for fit A is less likely

TABLE I. Parameters for polynomial fittings ( $a_1$ ,  $a_2$ , and  $a_3$ ) and fitting of the peak using Eq. (2) ( $\Lambda$ ,  $L$ ,  $f_0$ , and  $T_0$ ).

|     | $a_1$                 | $a_2$                 | $a_3$                 | $\Lambda$                   | $L$  | $f_0 = \frac{\omega_0}{2\pi}$ | $T_0$ |
|-----|-----------------------|-----------------------|-----------------------|-----------------------------|------|-------------------------------|-------|
| Fit | ( $\mu\text{J/K}^2$ ) | ( $\mu\text{J/K}^3$ ) | ( $\mu\text{J/K}^4$ ) | ( $10^{12}\text{cm}^{-2}$ ) | (nm) | (GHz)                         | (K)   |
| A   | 65                    |                       | 6400                  |                             |      |                               |       |
| B   | 20                    | 800                   | 4800                  | 4.4                         | 14   | 9.7                           | 0.46  |

to be correct compared with the 20% enhancement found for fit B. Therefore we conclude that fit B with the  $T^2$  term provides a better description of the data. This provides evidence of a 2D helium layer between amorphous and crystalline solid helium as seen in PIMC simulation studies [27]. The coefficient  $a_1$  in fit B is  $0.17 \mu\text{J/K}^2 \text{m}^2$  after being normalized by the surface area of silica strands. This is 20 times smaller than that for an amorphous  $^4\text{He}$  film at submonolayer coverage adsorbed from the vapor on silica substrate (Vycor) [36]. The large  $T$  linear heat capacity in Ref. [36] is associated with the excitations of atoms out of 2D adatom solid islands. Such excitations are suppressed in our samples when the system is filled with solid helium, giving a  $T$  linear term that is only contributed by TLS from the amorphous layer. On the other hand, the coefficient  $a_2$  in fit B, equivalent to  $6.7 \mu\text{J/K}^3 \text{m}^2$ , is close to that for a 2D solid ( $8.4 \mu\text{J/K}^3 \text{m}^2$ ) extracted from the heat capacity of full pore liquid  $^4\text{He}$  in Vycor where the ripplon excitations (also giving a heat capacity scaling with  $T^2$ ) are suppressed [36]. Based on  $a_2$ , we can deduce that the 2D Debye temperature is  $\Theta_{2D} = 25.7$  K. This is equivalent to the 2D solid with an areal density of  $n = 0.09 \text{ \AA}^{-2}$  according to the heat capacity measurement of solid  $^4\text{He}$  film on graphite [37]. The areal density gives an interatomic separation of  $3.56 \text{ \AA}$  assuming  $^4\text{He}$  atoms form honeycomb structure. It is 3% larger than the lattice constant in the basal plane for hcp solid helium [38], which means the 2D solid layer is less compact than three-dimensional (3D) crystalline solid.

The broad heat capacity peak with fit B subtracted is shown in Fig. 2(b). It shows characteristics different from the peak previously reported for bulk solid  $^4\text{He}$  samples [22–24]. The peak size of  $190 \mu\text{J/K mol}$  is 4 times larger than the largest peak reported for bulk samples and the position of the peak at 0.22 K is also a factor of 2 higher and more than twice higher than the purported NCRI onset (0.1 K) observed in torsional oscillator experiments for solid helium in aerogel [14]. A possible origin for the peak is the interaction between  $^3\text{He}$  impurities and dislocations or silica strands. The fact that the total heat capacity and the peak position are identical for the 0.3 ppm and 1 ppb samples [as shown in the inset of Fig. 2(a)] suggests that the  $^3\text{He}$  impurities in the 1 ppb sample have already saturated the effect and the size of the heat capacity translates to at least  $2 \times 10^4 k_B$  per  $^3\text{He}$  atom. This is unphysical.

Instead, we think a likely physical origin of the peak is the thermal excitation of the vibration of dislocations in solid helium. Dislocations can be treated as vibrating strings pinned at fixed nodes [39]. The vibration frequency is dependent on the length  $L$  of the dislocation line between the nodes with the wavelength of fundamental vibration mode equal to  $2L$ . For bulk solid  $^4\text{He}$  samples, the dislocation density  $\Lambda$  ranges from  $10^4$  to  $10^8 \text{ cm}^{-2}$  [16,40,41]. Assuming dislocations form an orthogonal 3D network,  $\Lambda$  and  $L$  satisfy the relation  $\Lambda L^2 \approx 3$  [40,41]. Therefore the value of  $L$  ranges from 1 to  $100 \mu\text{m}$ . With a typical value of  $L = 10 \mu\text{m}$ , the fundamental frequency is  $f_0 = \omega_0/2\pi = \frac{\sqrt{G/\rho}}{2L} = 13.7 \text{ MHz}$  corresponding to a characteristic temperature of  $T_0 = \hbar\omega_0/k_B = 0.65 \text{ mK}$ . Here  $G = 1.5 \times 10^7 \text{ Pa}$  is the shear modulus [42] and  $\rho = 0.2 \text{ g/cm}^3$  is the density for solid helium. Within the temperature range of our measurements (from 50 to 600 mK) the spectrum of

vibrational modes can be considered as continuous and its specific heat should scale with  $T$  [43]. Since  $\Lambda$  is relatively small and the vibration is populated by long-wavelength (low-energy) modes, the specific heat from dislocation is much smaller than the Debye specific heat and hard to observe. Specifically, for bulk solid helium, the ratio of the specific heat from dislocations to that from the Debye term is given by [43]

$$\frac{C_{\text{dis}}}{C_{\text{Debye}}} = \frac{5\Lambda a^2}{36\pi^2 Z} \left(\frac{\Theta_D}{T}\right)^2 = \frac{5.7 \times 10^{-9}}{(T [\text{K}])^2} \quad (1)$$

with  $\Lambda = 10^6 \text{ cm}^{-2}$ ,  $a = 3 \text{ \AA}$  is the lattice constant,  $Z = 2$  is the number of atoms per unit cell, and  $\Theta_D = 30 \text{ K}$  is the Debye temperature. The ratio decreases with increasing temperature and  $C_{\text{dis}}/C_{\text{Debye}} < 2.3 \times 10^{-6}$  for  $T > 50 \text{ mK}$ . Such a heat capacity contribution cannot be observed with our experimental resolution.

However, for solid helium grown in silica aerogel, the dislocation density is expected to be significantly increased by the interpenetrating network of the silica strands. Assuming a uniform average diameter of 5 nm for the silica strands and the strands form an orthogonal 3D network, the density of silica strands for an aerogel of 95% porosity is on the order of  $10^{12} \text{ cm}^{-2}$ . Lattice mismatch at interfaces is one of the main sources for the nucleation of dislocation line. Since there is obvious lattice mismatch between amorphous silica and solid helium, the silica strands, instead of the wall of the sample cell, become the main source that introduces dislocations. As a result the density of dislocation lines should be correlated with and be of the same order as the density of the silica strands. Therefore  $\Lambda$  is a factor of  $10^4$  to  $10^8$  larger than that found in bulk solid. In addition, due to the dense distribution of silica strands, dislocation lines starting from one strand have a large chance to be terminated at the nearest-neighboring strands. Considering the entanglement of dislocation lines themselves,  $L$  should not be larger than the separation of silica strands. Since the distance between the intersecting aerogel strands is  $30 \sim 100 \text{ nm}$  [44],  $L$  should also be distributed in the range close to or less than 30 nm. Therefore  $L$  is at least three orders of magnitude lower than that in bulk solid. As a result, the long-wavelength vibration modes of dislocations are cut off, forcing the fundamental mode to have shorter wavelength and higher energy. The characteristic temperature  $T_0$  also increases by three orders of magnitude approaching the highest temperature for which we have data. In this case only the fundamental mode makes a significant contribution to specific heat. As a result the specific heat is no longer linear in  $T$ . Instead it is given by [43]

$$C_{\text{dis}}(T) = \left(\frac{\Lambda}{L}\right) \left(\frac{a^3}{Z}\right) N k_B \left(\frac{\hbar\omega_0}{k_B T}\right)^2 e^{-\frac{\hbar\omega_0}{k_B T}}, \quad (2)$$

where  $N$  is the number of total helium atoms and  $k_B$  is Boltzmann constant. The solid line in Fig. 2(b) is the fitting of the peak by Eq. (2) with the fitting parameters listed in Table I. The fitting matches the peak size and position reasonably well and the fitting parameters ( $\Lambda = 4.4 \times 10^{12} \text{ cm}^{-2}$  and  $L = 14 \text{ nm}$ ) are in good agreement with the scenario that dislocations are pinned by silica strands. Moreover,  $T_0 = 0.46 \text{ K}$  justifies that only the fundamental mode needs to be considered. We note

that Eq. (2) does not fit the high-temperature side of the peak very well. If one makes the reasonable assumption that there should be a distribution for the value of  $L$ , then the fitting peak should be even broader. However, the discrepancy is less than 5% of the total measured heat capacity. The procedure in extracting the small difference (the peak) between two nearly similar quantities, i.e., the measured heat capacity and fit B, becomes progressively less reliable with increasing temperature. The fact that our model yields a peak with reasonable peak size and position allows us to conclude with a fair degree of confidence that the broad heat capacity peak we have observed is the consequence of the thermal activation of the vibrations of dislocations. The significant increase in  $\Lambda$  and the pinning of dislocations by silica strands make the heat capacity much more prominent than in bulk solids. To our knowledge this is the first observation of a thermodynamic signature of dislocation in solid helium and possibly in other crystalline solids.

#### IV. RESULTS ON $^3\text{He}$ - $^4\text{He}$ MIXTURE SAMPLES

Mixture samples with higher  $X_3$  are prepared with the following procedure. The calorimeter is kept above 20 K and continuously pumped for 2 days. The empty calorimeter is then cooled down to 20 mK. A desired quantity of  $^3\text{He}$  is dosed into the calorimeter. The dosage is calculated based on the density and volume of the solid and the desired  $X_3$ . UHP  $^4\text{He}$  is then condensed into the calorimeter and frozen into solid phase. Eight mixture samples are made with  $X_3$  ranging from 6 ppm to 1.4%.

The results of solid  $^3\text{He}$ - $^4\text{He}$  mixture samples are shown in Fig. 3. The 1% and 1.4% samples have extremely long thermal equilibrium time constants at low temperatures because of their large heat capacities. The time constants drastically increase with decreasing temperature from  $\sim 0.5$  hours at 0.6 K to  $\sim 6$  hours at 0.2 K, and on these samples it is impractical to do measurement below 0.15 K. The heat capacity curves for the mixture samples collapse onto that for the pure  $^4\text{He}$  samples at high temperature but show a significant enhancement below

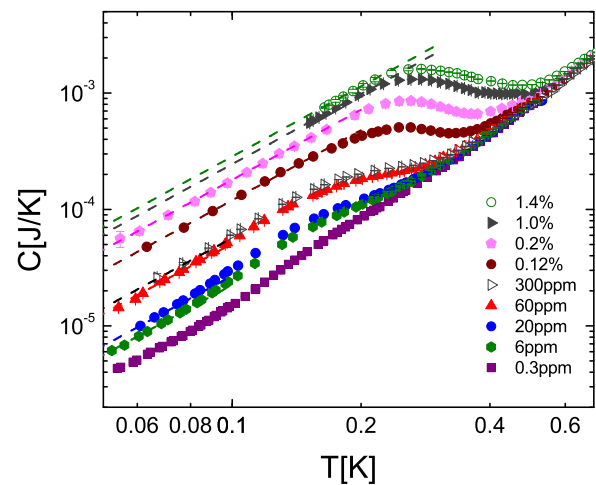


FIG. 3. (Color online) Heat capacities of solid  $^3\text{He}$ - $^4\text{He}$  mixture samples grown in aerogel. The dashed lines show the  $T^2$  dependence of the enhanced heat capacities at low temperature.

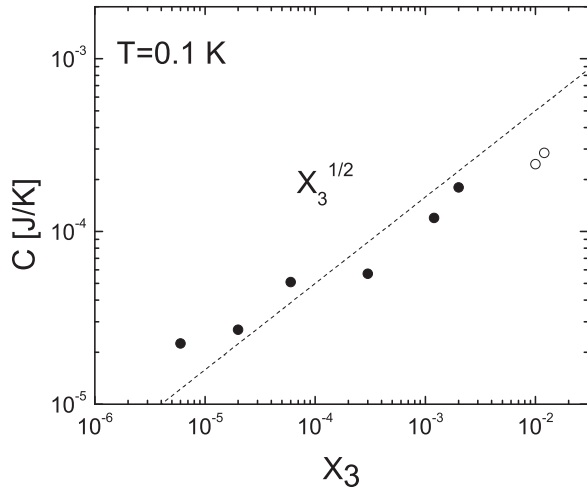


FIG. 4.  $X_3$  dependence of the enhanced heat capacity at  $T = 0.1$  K. The dashed line represents  $X_3^{1/2}$  dependence. The open symbols represent the extrapolated values for 1.0% and 1.4% samples.

a characteristic temperature  $T_c$ .  $T_c$  increases from 0.32 to 0.62 K as  $X_3$  is increased from 6 ppm to 1.4%. The heat capacities of all the mixture samples appear to scale with  $X_3^{1/2}$  at fixed temperature (the extrapolated values for 1% and 1.4% samples also obey this dependence) and  $T^2$  at fixed  $X_3$  below 0.15 K. These dependencies are shown in Fig. 4 and Fig. 3. No hysteresis was observed between the data taken during warming and cooling processes.

The results for our mixture samples in aerogel resemble the heat capacity results of bulk solid mixtures. Edwards, McWilliams, and Daunt (EMD) measured the heat capacity of bulk solid  $^3\text{He}$ - $^4\text{He}$  mixture and found a large heat capacity enhancement in addition to a  $T^3$  term below phase separation temperature  $T_{PS}$  [45]. Their extra heat capacity originates from 3D phase separation of  $^3\text{He}$ - $^4\text{He}$  mixture and is in good agreement with theories [46,47]. There are, however, three significant differences between the EMD results and ours. First, the EMD results with different mixture ratios collapse onto one common envelop below  $T_{PS}$  while ours scale with  $X_3^{1/2}$ . Second, the EMD results show that the extra heat capacity is 100 ~ 1000 times larger than the  $T^3$  term. Our largest heat capacity enhancement with  $X_3 = 1.4\%$  is only 20 times larger than that for the pure  $^4\text{He}$  samples. Third,  $T_c$  for the mixture samples in aerogel is significantly higher than  $T_{PS}$  for mixture samples without aerogel. Specifically,  $T_{PS}$  was found below 0.17 K for samples with impurity concentration less than 1.4% [46]. Inside aerogel,  $T_c$  ranges from 0.32 K to 0.62 K for  $X_3$  that ranges from 6 ppm to 1.4%. In addition, in contrast to previous heat capacity studies of bulk mixtures [23], within the resolution of our experiment, we do not find any evidence of hysteresis in the heat capacity data upon warming and cooling of the mixture sample confined in aerogel. We believe the differences between our results and those for bulk mixture samples are due to the fact that the large surface area of the silica strands provides readily available low potential energy sites to accommodate  $^3\text{He}$  atoms and hence a well-defined low-energy configuration that facilitates the

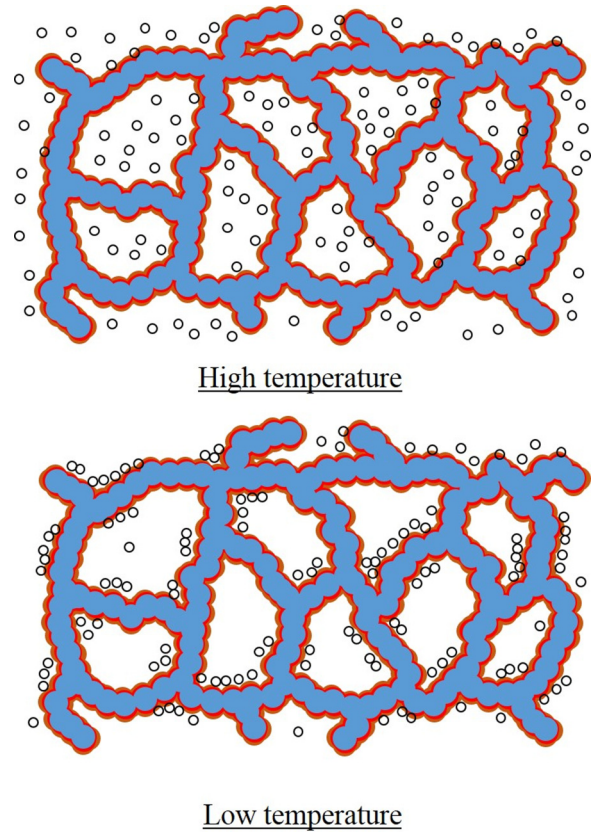


FIG. 5. (Color online) Distribution of  $^3\text{He}$  atoms in solid  $^4\text{He}$  grown in aerogel. Silica strands (light blue) are coated by strongly localized amorphous layer of  $^4\text{He}$  (brown).  $^3\text{He}$  atoms (black circle) are evenly distributed in crystalline grains of  $^4\text{He}$  (in the pore space, not shown) at high temperature and bind to the intermediate layer at low temperature.

phase separation process below the characteristic temperature  $T_c$ . This is not the case for bulk mixtures without the aerogel.

As noted above, for pure  $^4\text{He}$  samples the strong van der Waals attraction from silica induces the formation of a strongly bound amorphous layer of  $^4\text{He}$ . This dense amorphous layer will remain to be pure  $^4\text{He}$  even when the pure  $^4\text{He}$  sample is replaced by mixture samples because the larger zero-point energy of the  $^3\text{He}$  atoms favors them to be located away from the silica surface. At high temperature,  $^3\text{He}$  atoms are evenly distributed in the crystalline grains in the pore space. At low temperature,  $^3\text{He}$  atoms are expelled from the  $^4\text{He}$  crystallite and as shown by the PIMC simulation [27] the position with the lowest potential energy for a  $^3\text{He}$  atom lies immediately outside the amorphous surface layer. As a result, the phase-separated  $^3\text{He}$  atoms will reside on the intermediate layer on top of the strongly bound amorphous  $^4\text{He}$  layer as depicted in Fig. 5.

We can estimate the spatial distribution of  $^3\text{He}$  as a function of temperature. A simple calculation based on the specific surface area and porosity of aerogel shows that one complete monolayer enclosing the entire surface of silica strands can accommodate 3% of all helium atoms in the sample cell. The dense amorphous surface layer therefore accounts for 6% of all the  $^4\text{He}$  atoms in the sample with the  $^3\text{He}$  atoms distributed in the intermediate layer and the crystalline grains. These two

regions account for 3% and 91% of the total number of  $^3\text{He}$  and  $^4\text{He}$  atoms ( $N$ ) in a mixture sample, respectively. The fraction of  $^3\text{He}$  binding to the intermediate layer (with binding energy  $E_b = -0.8$  K [27]) is  $n_{3\text{bind}}/n_3$ . This fraction is given by  $n_{3\text{bind}}/n_3 = (N_{\text{int}}e^{-E_b/T})/(N_{\text{int}}e^{-E_b/T} + N_{\text{cryst}})$ , where  $N_{\text{int}}$  and  $N_{\text{cryst}}$  are the total number of sites available for  $^3\text{He}$  (and  $^4\text{He}$ ) atoms in the intermediate layer and crystalline grains. As mentioned above,  $N_{\text{int}} \approx 0.03N$  and  $N_{\text{cryst}} \approx 0.91N$ . Since  $E_b = -0.8$  K,  $n_{3\text{bind}}/n_3$  rapidly increases towards unity as  $T$  is decreased from 0.6 K to lower temperatures. The temperature region for the rapid increase of  $n_{3\text{bind}}/n_3$  is consistent with the range of  $T_c$  between 0.32 to 0.62 K found for the mixture samples.

The enhanced heat capacities at low temperature exhibit  $T^2$  dependence at fixed  $X_3$  and  $X_3^{1/2}$  dependence at fixed  $T$ . We will discuss the possible physical origin of these two dependencies in the rest of this paper.

The PIMC simulation suggests that the intermediate layer is liquid. As mentioned above, our experimental results for the pure  $^4\text{He}$  samples do not support this conclusion and the results for the mixture samples also do not give any evidence of a 2D liquid  $^3\text{He}$  layer. If the  $^3\text{He}$  atoms form 2D liquid in the intermediate layer, we should observe a heat capacity consistent with that for a 2D Fermi liquid:  $C_{\text{fermi}} = \frac{\pi k_B^2}{3\hbar^2} m^* S T$ , where  $m^*$  is the effective mass of  $^3\text{He}$  (experimentally determined to be  $1.7m_3$  [48];  $m_3$  is the mass of  $^3\text{He}$  atom) and  $S$  the area of 2D liquid  $^3\text{He}$ . This is not consistent with our measurements that the heat capacities scale with  $T^2$ . It is tempting to attribute the  $T^2$  dependence to be the consequence of a 2D phonon contribution. However, there is difficulty with this attribution. Specifically the magnitude of the  $T^2$  term found for these  $^3\text{He}$  patches is exceptionally large as compared with that found in 2D  $^4\text{He}$  layers reported above. It is 1.5 times larger for the 6 ppm sample and 20 times larger for the 1.4% sample. Since the  $^3\text{He}$  atom is only 25% lighter than the  $^4\text{He}$  atom, it cannot lead to a large increase in 2D Debye heat capacity as in our observation. This large discrepancy indicates 2D phonons cannot be the sole explanation for the observed heat capacity.

On the other hand, the  $X_3^{1/2}$  dependence suggests that the phase-separated  $^3\text{He}$  atoms are favored to form isotopically pure and atomically thin patches at local potential minima within the intermediate layer and there exist excitations of  $^3\text{He}$ - $^4\text{He}$  exchange at the patch perimeters. The attractive potential entraining the  $^3\text{He}$  layer on top of the amorphous  $^4\text{He}$  layer is not completely uniform at the atomic scale and the  $^3\text{He}$  patches will nucleate at positions of local potential minima. While phase separated, it is energetically more favorable for the  $^3\text{He}$  atoms at and near the perimeters of the patches to interact and undergo exchange with the adjacent  $^4\text{He}$  atoms in the same intermediate layer than those either in the dense

amorphous surface layer or in the crystallites. Since these excitations happen at the boundaries between  $^3\text{He}$  and  $^4\text{He}$  patches, the enhanced heat capacity scales with the total length of the perimeters. For samples with low  $X_3$ , the  $^3\text{He}$  patches form at local potential minima and the number of patches is constant. In this  $X_3$  range, the length of perimeters scales with  $X_3^{1/2}$ . As coverage (or  $X_3$ ) is increased, individual patches start to merge and the total number of  $^3\text{He}$  patches decreases. As a result, the increase of total length of the perimeters is slower than the increase of  $X_3^{1/2}$ . This may be the reason that the heat capacities of samples with higher  $X_3$  fall below the  $X_3^{1/2}$  dependence as seen in Fig. 4.

While we are confident that our heat capacity data provide strong evidence of phase separation of  $^3\text{He}$  of the mixture samples at low temperature and the phase-separated  $^3\text{He}$  form 2D solid patches in the intermediate layer conforming to the surface of the aerogel strands, we are unable to come up with a more precise physical model that explains simultaneously the  $T^2$  dependence at a fixed  $X_3$  and the  $X_3^{1/2}$  dependence at a fixed temperature. Additional experimental probes such as NMR study of  $^3\text{He}$  [9,49,50] may be useful to clarify this puzzle.

## V. CONCLUSIONS

In conclusion, we have measured the heat capacity of solid  $^4\text{He}$  and solid  $^3\text{He}$ - $^4\text{He}$  mixtures grown in aerogel. The heat capacity of solid  $^4\text{He}$  samples shows a broad peak between 0.1 and 0.35 K in addition to regular polynomial background in the form of  $a_1T + a_2T^2 + a_3T^3$ . The polynomial terms indicate that the layer of helium in contact with silica strands is amorphous and most of helium atoms far away from silica strands form crystalline grains. The helium atoms sandwiched by these two parts form a distinct 2D solid layer. The broad peak might have its origin in the vibration of dislocation lines which are pinned by silica strands. Heat capacities of the mixture samples show evidence of phase separation of the  $^3\text{He}$  atoms at low temperatures. Below a characteristic phase separation temperature that increases with  $^3\text{He}$  concentration, the  $^3\text{He}$  atoms form 2D solid patches in the intermediate layer sandwiched between the amorphous layer and  $^4\text{He}$  crystallites. The excitations of  $^3\text{He}$ - $^4\text{He}$  exchange at the perimeters of the  $^3\text{He}$  patches give rise to the  $X_3^{1/2}$  dependence of the measured heat capacity below 0.15 K.

## ACKNOWLEDGMENTS

We acknowledge John Beamish and Milton Cole for helpful discussions and John Beamish for making available the isotopically pure  $^4\text{He}$ . This research was supported by NSF Grant No. DMR1103159.

- 
- [1] E. Kim and M. H. W. Chan, *Science* **305**, 1941 (2004).  
 [2] E. Kim and M. H. W. Chan, *Nature (London)* **427**, 225 (2004).  
 [3] M. Kondo, S. Takada, Y. Shibayama, and K. Shirahama, *J. Low Temp. Phys.* **148**, 695 (2007).

- [4] Y. Aoki, J. C. Graves, and H. Kojima, *Phys. Rev. Lett.* **99**, 015301 (2007).  
 [5] A. S. C. Rittner and J. D. Reppy, *Phys. Rev. Lett.* **98**, 175302 (2007).

- [6] A. Penzev, Y. Yasuta, and M. Kubota, *Phys. Rev. Lett.* **101**, 065301 (2008).
- [7] B. Hunt, E. Pratt, V. Gadagkar, M. Yamashita, A. V. Balatsky, and J. C. Davis, *Science* **324**, 632 (2009).
- [8] D. Y. Kim, S. Kwon, H. Choi, H. C. Kim, and E. Kim, *New J. Phys.* **12**, 033004 (2010).
- [9] R. Toda, P. Gumann, K. Kosaka, M. Kanemoto, W. Onoe, and Y. Sasaki, *Phys. Rev. B* **81**, 214515 (2010).
- [10] A. Eyal, O. Pelleg, L. Embon, and E. Polturak, *Phys. Rev. Lett.* **105**, 025301 (2010).
- [11] D. E. Zmееv and A. I. Golov, *Phys. Rev. Lett.* **107**, 065302 (2011).
- [12] A. D. Fefferman, X. Rojas, A. Haziот, S. Balibar, J. T. West, and M. H. W. Chan, *Phys. Rev. B* **85**, 094103 (2012).
- [13] G. Nichols, M. Poole, J. Nyeki, J. Saunders, and B. Cowan, [arXiv:1311.3110](https://arxiv.org/abs/1311.3110).
- [14] N. Mulders, J. T. West, M. H. W. Chan, C. N. Kodituwakku, C. A. Burns, and L. B. Lurio, *Phys. Rev. Lett.* **101**, 165303 (2008).
- [15] J. Day and J. R. Beamish, *Nature (London)* **450**, 853 (2007).
- [16] A. Haziот, X. Rojas, A. D. Fefferman, J. R. Beamish, and S. Balibar, *Phys. Rev. Lett.* **110**, 035301 (2013).
- [17] J. R. Beamish, A. D. Fefferman, A. Haziот, X. Rojas, and S. Balibar, *Phys. Rev. B* **85**, 180501 (2012).
- [18] H. J. Maris, *Phys. Rev. B* **86**, 020502 (2012).
- [19] D. Y. Kim, J. T. West, T. A. Engstrom, N. Mulders, and M. H. W. Chan, *Phys. Rev. B* **85**, 024533 (2012).
- [20] D. Y. Kim and M. H. W. Chan, *Phys. Rev. B* **90**, 064503 (2014).
- [21] D. Y. Kim and M. H. W. Chan, *Phys. Rev. Lett.* **109**, 155301 (2012).
- [22] X. Lin, A. C. Clark, and M. H. W. Chan, *Nature (London)* **449**, 1025 (2007).
- [23] X. Lin, A. C. Clark, Z. G. Cheng, and M. H. W. Chan, *Phys. Rev. Lett.* **102**, 125302 (2009).
- [24] J. T. West, X. Lin, Z. G. Cheng, and M. H. W. Chan, *Phys. Rev. Lett.* **102**, 185302 (2009).
- [25] Z. G. Cheng *et al.* (unpublished).
- [26] E. S. Sabisky and C. H. Anderson, *Phys. Rev. Lett.* **30**, 1122 (1973).
- [27] S. A. Khairallah and D. M. Ceperley, *Phys. Rev. Lett.* **95**, 185301 (2005).
- [28] D. Wallacher, M. Rheinstaedter, T. Hansen, and K. Knorr, *J. Low Temp. Phys.* **138**, 1013 (2005).
- [29] D. W. Schaefer and K. D. Keefer, *Phys. Rev. Lett.* **56**, 2199 (1986).
- [30] R. Vacher, T. Woignier, J. Pelous, and E. Courtens, *Phys. Rev. B* **37**, 6500 (1988).
- [31] P. W. Anderson, B. I. Halperin, and C. M. Varma, *Philos. Mag.* **25**, 1 (1972).
- [32] W. A. Phillips, *J. Low Temp. Phys.* **7**, 351 (1972).
- [33] E. C. Heltemes and C. A. Swenson, *Phys. Rev. Lett.* **7**, 363 (1961).
- [34] E. C. Heltemes and C. A. Swenson, *Phys. Rev.* **128**, 1512 (1962).
- [35] C. N. King, W. A. Phillips, and J. P. de Neufville, *Phys. Rev. Lett.* **32**, 538 (1974).
- [36] R. H. Tait and J. D. Reppy, *Phys. Rev. B* **20**, 997 (1979).
- [37] M. Bretz, J. G. Dash, D. C. Hickernell, E. O. McLean, and O. E. Vilches, *Phys. Rev. A* **8**, 1589 (1973).
- [38] J. Donohue, *Phys. Rev.* **114**, 1009 (1959).
- [39] A. Granato and K. Lücke, *J. Appl. Phys.* **27**, 583 (1956).
- [40] I. Iwasa and H. Suzuki, *J. Phys. Soc. Jpn.* **49**, 1722 (1980).
- [41] A. Haziот, A. D. Fefferman, J. R. Beamish, and S. Balibar, *Phys. Rev. B* **87**, 060509 (2013).
- [42] J. Beamish, *J. Low Temp. Phys.* **168**, 194 (2012).
- [43] A. Granato, *Phys. Rev.* **111**, 740 (1958).
- [44] W. P. Halperin and J. A. Sauls, [arXiv:cond-mat/0408593](https://arxiv.org/abs/cond-mat/0408593).
- [45] D. O. Edwards, A. S. McWilliams, and J. G. Daunt, *Phys. Rev. Lett.* **9**, 195 (1962).
- [46] D. O. Edwards and S. Balibar, *Phys. Rev. B* **39**, 4083 (1989).
- [47] D. O. Edwards and M. S. Pettersen, *J. Low Temp. Phys.* **87**, 473 (1992).
- [48] B. Bhattacharyya and F. M. Gasparini, *Phys. Rev. Lett.* **49**, 919 (1982).
- [49] S. S. Kim, C. Huan, L. Yin, J. Xia, D. Candela, and N. S. Sullivan, *Phys. Rev. Lett.* **106**, 185303 (2011).
- [50] S. S. Kim, C. Huan, L. Yin, J. S. Xia, D. Candela, and N. S. Sullivan, *Phys. Rev. B* **87**, 224303 (2013).